The Meteoritical Society

Meteoritics & Planetary Science 45, Nr 8, 1284–1301 (2010)
doi: 10.1111/j.1945-5100.2010.01085.x

Pyroclast loss or retention during explosive volcanism on asteroids: Influence of asteroid size and gas content of melt

Lionel WILSON[1*], Klaus KEIL[2], and Timothy J. McCOY[3]

[1]Lancaster Environment Centre, Lancaster University, Lancaster LA1 4YQ, UK
[2]Hawaii Institute of Geophysics and Planetology, School of Ocean and Earth Science and Technology, University of Hawaii at Manoa, Honolulu, Hawaii 96822, USA
[3]Department of Mineral Sciences, National Museum of Natural History, Smithsonian Institution, Washington, D.C. 20560–0119, USA
[*]Corresponding author. E-mail: l.wilson@lancaster.ac.uk

(Received 24 May 2010; revision accepted 31 May 2010)

Abstract–We review the conditions under which explosive volcanism took place on early-forming differentiated asteroids. The pressure-dependent solubility of typical asteroid volatiles in melts implies that the gas driving explosive volcanism on asteroids less than approximately 100 km in diameter was probably present mainly as a free phase capable of accumulating into large gas bodies and, thus, causing slug flow in melts approaching the surface. In contrast, in asteroids larger than approximately 100 km the gas was probably present largely as a dispersion of small bubbles. We show that these gas distributions have implications for the size distribution of the pyroclastic droplets produced in explosive eruptions at the surface. All pyroclastic melt droplets are accelerated by the expanding gases, but their speeds lag the gas speed by a finite amount that is a function of the droplet size and density and the asteroid size and, hence, acceleration due to gravity. We compute pyroclast speeds and, by comparing them with escape velocities, we identify the critical pyroclast diameter on a given-size asteroid that distinguishes droplets lost to space from droplets that return to the surface. Identification of asteroidal pyroclasts and measurements of their sizes could throw light on the amounts of gas driving eruptions.

INTRODUCTION

Since the recognition that pyroclastic volcanism was an important process in the early differentiation of asteroids (Wilson and Keil 1991), the role that this process has played on a wide range of differentiated meteorite parent bodies has been explored. These include the explosive ejection of silicate pyroclasts to explain the near-complete absence of basaltic crusts on the fairly small aubrite and ureilite parent bodies (Wilson and Keil 1991, 1996a; Muenow et al. 1992; Warren and Kallemeyn 1992; Goodrich et al. 2007; Wilson et al. 2008); the explosive ejection of early metallic Fe,Ni–FeS melts at greater than escape velocity as a way of understanding the metal to sulfur ratio in numerous families of iron meteorites (Keil and Wilson 1993; McCoy et al. 2006); the extent to which sulfide and silicate melt segregation occurs as a function of the extent of partial melting (McCoy et al. 1997a, 1997b); and the relative importance of shallow silicate magma intrusion, the eruption of this magma as surface lava flows, and accumulation of silicate pyroclasts on the relatively large asteroid 4 Vesta (Wilson and Keil 1996b, 1997).

No examples exist of extensive pyroclastic deposits sampled by meteorites derived from differentiated asteroids. This is readily understandable in relation to meteorite suites such as the aubrites and ureilites, which appear to originate from parent bodies small enough that essentially all pyroclasts were ejected with escape velocity (Wilson and Keil 1991; Warren and Kallemeyn 1992). At first sight, it is less clear why the howardites, eucrites, and diogenites (HED) suite, assumed to be derived from 4 Vesta, an asteroid large enough to be

expected to have retained pyroclasts (Wilson and Keil 1996b), should be devoid of pyroclasts. However, Wilson and Keil (1997) showed that the small sizes expected for pyroclasts erupted on a body with negligible atmosphere, coupled with the relatively large acceleration due to gravity on 4 Vesta, would lead to almost all of the pyroclasts from an explosive eruption forming an optically dense fire fountain over the vent. The vast majority of pyroclasts would fall from the fountain without appreciable cooling and accumulate to form a lava pond. After it had cooled, the resulting rock would be indistinguishable from a lava flow deposit. Thus in general, the lack of meteorites containing pyroclasts is understandable.

For the above reasons, previous treatments of explosive asteroid volcanism have been polarized between eruptions on bodies small enough that essentially all of the pyroclasts are likely to be erupted at greater than escape velocity and lost into space, and eruptions on bodies large enough that essentially all of the pyroclasts are likely to be retained. Here, we focus on activity on a wide range of asteroid sizes, exploring the circumstances where the size distribution of pyroclasts and the volatile content of the magma may be such that the smaller pyroclasts are ejected with greater than escape velocity but the larger ones, having a significant terminal fall velocity through the released volcanic gas, do not escape but instead eventually fall back to the surface. This study is prompted by the discovery (McCoy and Gale 2006) of a pair of centimeter-sized clasts with igneous contacts between them, one a silicate vitrophyre and one of metallic Fe,Ni–FeS composition, in the aubrite meteorite Larkman Nunatak (LAR) 04316. The Fe,Ni–FeS clast is a type previously unknown in aubrites; the silicate clast is similar in composition to the rare and smaller clasts described by Fogel (2005) from the Parsa enstatite chondrite and the Khor Temiki and Lewis Cliff (LEW) 87007 aubrites. Although it has been suggested that the Parsa (Nehru et al. 1984) and Khor Temiki clasts (Keil 2007) may be impact melts, the association and sizes of the new LAR 04316 clasts warrant examination of the possibility that they are examples of pyroclasts retained on their parent body because of their large sizes as it lost almost all of its pyroclastic material to space.

Many aspects of melt formation and migration in asteroids have already been developed (Muenow et al. 1992; Keil and Wilson 1993; Wilson and Keil 1996b; Wilson et al. 2008). We briefly summarize relevant earlier work as required, but focus mainly on the issues previously not considered in detail, especially the consequences of the way volatiles are distributed in molten silicates and sulfides, as dissolved species or as free gases. This strongly influences the size distribution of the pyroclastic droplets that are eventually produced. We also explore in detail the critical pyroclast size, for a given melt density, asteroid size, and melt volatile content, that marks the boundary between loss into space and retention on the surface.

MELTING IN ASTEROIDS

Although localized heating due to impacts, especially during accretion, must have contributed in part to the thermal budgets of asteroids, impacts large enough to cause large-scale melting in small bodies would have caused their disruption (Keil et al. 1997). Electrical conduction heating by the T Tauri-phase solar wind (Sonett et al. 1970) remains a possible source, but the most likely heat source able to explain partial silicate melting in small asteroids is the decay of short-lived ^{26}Al with a half-life of 0.72 Ma (e.g., Urey 1955; Srinivasan et al. 1999; Nyquist et al. 2001; McCoy et al. 2006). The progressive removal from the interior of Al partitioned into basaltic melts that migrate toward the surface, however, may have limited the ability of ^{26}Al to cause complete melting. Shukolyukov and Lugmair (1993) and Tachibana and Huss (2003), for example, suggested that short-lived ^{60}Fe with a half-life of 1.5 Ma may also have played a significant role in the melting of differentiated asteroids, although Ghosh et al. (2006) calculate that, for the most realistic estimates of initial ^{60}Fe/^{56}Fe ratios, the rate of heat generation at the time of calcium-aluminum-rich inclusions (CAI) formation is 2–4 orders of magnitude smaller for ^{60}Fe than for ^{26}Al, which makes it questionable that ^{60}Fe could have been an important heat source in the melting of asteroids.

The short half-life of ^{26}Al controls the combinations of size and formation time of asteroids for which it can be an important heat source. Furthermore, such asteroids must heat up rapidly and nearly isothermally. This is because rapid heat generation inside any roughly spherical asteroidal or planetary body in which solid-state convection is absent or minimal, so that heat transfer is dominated by the inefficient process of conduction, must lead to a very shallow temperature gradient in the deep interior, grading rapidly into a very steep temperature gradient in an outer shell. The thickness of this outer shell (see, e.g., fig. 32 in Carslaw and Jaeger 1959) is close to $[3\ (\kappa\tau)^{1/2}]$, where κ is the thermal diffusivity of the asteroid rock and τ the time since asteroid formation. The period of time for which a significant heat source can be present is a few times the half-life of ^{26}Al, approximately 2.26×10^{13} s (Norris et al. 1983; Wu and Browne 1998), i.e., approximately 10^{14} s which equates to a few Ma. The thermal diffusivity of all solid silicates at the relevant

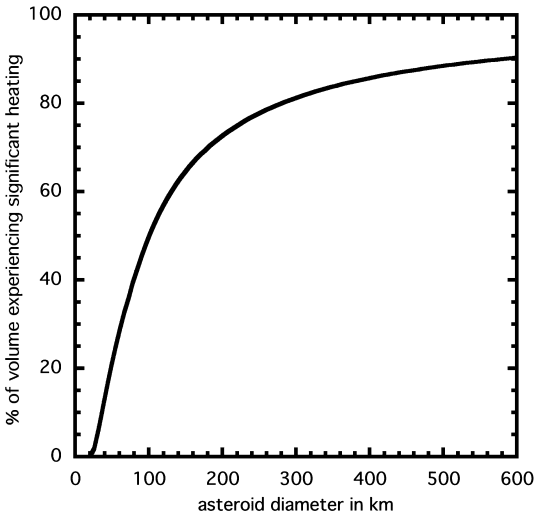

Fig. 1. Percentage of the total volume of an asteroid of a given diameter that experiences essentially uniform heating.

temperatures is approximately 7×10^{-7} m^2 s^{-1} (Whittington et al. 2009); however, Warren (2010) has pointed out that in the fragmental regoliths or mega-regoliths of asteroids a more appropriate value may be approximately 1×10^{-7} m^2 s^{-1}. The shell thickness by the time significant heating has taken place in an asteroid accreting very soon after CAI formation is therefore approximately 5–10 km. Thus, no asteroid smaller than approximately 10 km in diameter will have experienced significant internal heating, essentially irrespective of how early it formed.

Figure 1 shows the percentage of the volume of the body undergoing significant heating as a function of the asteroid diameter for sizes up to that of 4 Vesta, the largest asteroid for which we have evidence for internal silicate melting (e.g., Burbine et al. 2002). For all asteroids more than approximately 30 km in diameter the maximum temperature, and hence the maximum amount of melting that can be achieved, depends much more strongly on the time of asteroid formation than the asteroid size. Wilson et al. (2008) showed that the approximately 100 km diameter ureilite parent body was able to achieve the approximately 30% melting implied by the mineralogy of the ureilite meteorites if it accreted at approximately 0.55 Ma after CAI formation, the maximum temperature being reached at approximately 5 Ma after formation. Earlier formation leads to a higher maximum temperature, with the maximum being achieved sooner. Complete melting of the interior is theoretically possible with sufficiently early accretion, and estimates of the actual extent of melting must come from meteorite evidence (McCoy et al. 2006).

Table 1. Variation of pressures with asteroid diameter.

D	P_{10}	P_0
40	0.46	0.61
60	0.76	1.37
80	1.07	2.43
100	1.37	3.80
120	1.67	5.48
140	1.98	7.45
160	2.28	9.74
180	2.59	12.32
200	2.89	15.21
300	4.41	34.23
400	5.93	60.85
500	7.45	95.08
600	8.98	136.91

Note: D is the diameter of the asteroid in km; P_{10} is the pressure in MPa at the base of the conductively cooled crust at approximately 10 km depth; P_0 is the pressure in MPa at the center of the asteroid.

VOLATILES AVAILABLE FOR ASTEROID VOLCANISM

Any general treatment of explosive volcanic activity requires three kinds of input information: the likely composition, specifically the average molecular mass, m, of the volatiles; the mass fractions, n_m, of the melts that the volatiles represent; and the physical disposition of the volatiles—dissolved in the melt phases or present as free gas phases in pore space or fractures. We now review the available evidence on these issues as it relates to asteroids.

The many differentiated meteorite types of asteroidal origin (see Table 1 in Mittlefehldt et al. 1998) have experienced varying degrees of partial melting, melt migration, and possibly volcanism. For some of these differentiated meteorites, suggestions have been made as to their parent lithologies from which they formed by partial melting, differentiation and fractional crystallization, and measurements have been made of volatiles in proxies of these potential parent lithologies to estimate their role in volcanic processes. For example, the aubrites are thought to have formed by the melting, fractionation and differentiation of enstatite chondrite-like precursor lithologies, as is likely in view of the compositional and isotopic similarities of aubrites and enstatite chondrites (e.g., Keil, Forthcoming, 1989). Therefore, Muenow et al. (1992) measured indigeneous volatiles released at $T > 1200$ K from enstatite chondrites as a proxy for the parent lithologies of the aubrites. They found that species not attributable to terrestrial contamination of the meteorites examined included CO (1580–2830 ppm), N_2 (110–430 ppm), and Cl (120–450 ppm). Note that the entire amount of S could not be removed in the Muenow et al. (1992)

degassing experiments due to the upper temperature limit of the furnace of 1550 K. Based on the total S content of Indarch, 5.78 wt%, and of Hvittis, 3.30 wt% (Keil 1968), the amount of S released in the degassing experiments ranges from 15.5% of the total sulfur for Indarch to 48.0% for Hvittis, implying values of n from 10,115 to 15,840 ppm. The sources of these volatiles are not easily identifiable: some volatiles may have been trapped from the time of formation of the asteroid in pore spaces and cracks in minerals and clasts, whereas others may be produced by thermal decomposition or chemical reactions.

Furthermore, the ureilites are thought to have formed by the partial melting of some kind of carbonaceous chondrite, perhaps CV-type chondrites (e.g., Mittlefehldt et al. 1998). It has been proposed that copious amounts of CO were produced by a smelting reaction between graphite and FeO-bearing silicates during partial melting of the precursor carbonaceous chondrite lithology, and CO is implicated as the major volatile source in the ureilite parent body during partial melting and fractionation that may have driven explosive pyroclastic volcanism (Goodrich et al. 2007). These authors proposed that as much as 20% by mass (i.e., 200,000 ppm) of CO may have been available during the main silicate melting period.

Another example is provided by the acapulcoites–lodranites, which are residues of partial melting of ordinary chondrite-like precursor lithologies, with the acapulcoites representing low degrees and the lodranites higher degrees of partial melting of <1 to >20 vol% (McCoy et al. 1996, 1997a). These rocks present evidence for melt migration, and their parent body may have experienced pyroclastic volcanism. Muenow et al. (1995) carried out dynamic high-temperature mass spectrometry of seven unequilibrated ordinary chondrites as proxies for the parent lithologies of the acapulcoites–lodranites. They found that between 1020 and 1570 K, the following indigeneous volatiles were released: CO (245–8550 ppm), CO_2 (50–480 ppm), and Cl (380–455 ppm). Furthermore, McCoy et al. (1997b) used the same high-temperature mass spectrometry to determine the amounts of indigenous volatiles in the meteorites Acapulco and Lodran and found CO (up to 630 ppm), CO_2 ($\sim$100 ppm), S_2 ($>$10,000 ppm), Cl (250 ppm), and Na ($\sim$1000 ppm).

Given the molecular masses of the commonest of the above volatiles ($\sim$28, 28, 35, 44, and 64 kg kmol^{-1} for CO, N_2, Cl, CO_2, and S_2, respectively), the value used in our subsequent calculations for the mean molecular mass is $m = 40$ kg kmol^{-1}, with the caveat that the actual value could differ from this, in an extreme case, by as much as 60%. We address the consequences of assuming different values of m at the end of the analysis.

The meteorites from which the above evidence on volatile amounts is obtained were extracted from their parent bodies by impacts. The impact process is likely to have provided the opportunity for volatile loss, and so the measured volatile contents might be lower limits. Estimates of the maximum possible prevolcanism contents of physically trapped volatiles can be derived by considering the porosities of asteroids. Combining asteroid masses and volumes suggests that bodies as large as 4 Vesta have inherent small-scale porosities, f, of approximately 10%, the value rising to approximately 30% for bodies approximately 100 km in diameter (Britt et al. 2002). If these pore spaces contain free gases, we can determine the mass fraction of the asteroid that the gases represent if the gas pressure and temperature are known. The conditions of interest are those just prior to sulfide melting but after thermal metamorphism. The temperature, T_s, will then be approximately 1253 K, the Fe,Ni–FeS cotectic temperature (Kullerud 1963) and the pressure is likely to approximate the lithostatic pressure, P, which, at depth d below the surface of an asteroid of diameter D and uniform density ρ_a is given by

$$P = \frac{2}{3}\pi G \rho_a^2 \left(d D - d^2\right), \quad (1)$$

where G is the universal gravitation constant, 6.67×10^{-11} m^3 s^{-2} kg^{-1}. Table 1 shows a selection of pressures at 10 km depth, P_{10}, and at the centers, P_0, of asteroids with a range of diameters when the bulk density of the body is 3300 kg m^{-3}. Values range from a few MPa to more than 100 MPa. Using the perfect gas law to relate the gas density ρ_g to the pressure, P, and temperature T_s:

$$\rho_g = \frac{m P}{Q T_s}, \quad (2)$$

where Q is the universal gas constant, 8.314 J mol^{-1} K^{-1}. If n is the mass fraction of the asteroid that consists of the trapped volatiles, the partial volume v_g occupied by the gas is proportional to (n/ρ_g) and the partial volume v_s of the surrounding solid material is proportional to $[(1 - n)/\rho_a]$. By definition the porosity f must be equal to $[v_g/(v_g + v_s)]$, and so we find

$$n = \frac{f m P}{Q T_s \rho_a (1 - f) + f m P}. \quad (3)$$

Figure 2 shows how n varies with f and P over the ranges of values specified above. Note that pressures in the deep interiors of asteroids more than approximately 100 km in diameter exceed the critical pressures of most of the gas species mentioned above, and so the gas law

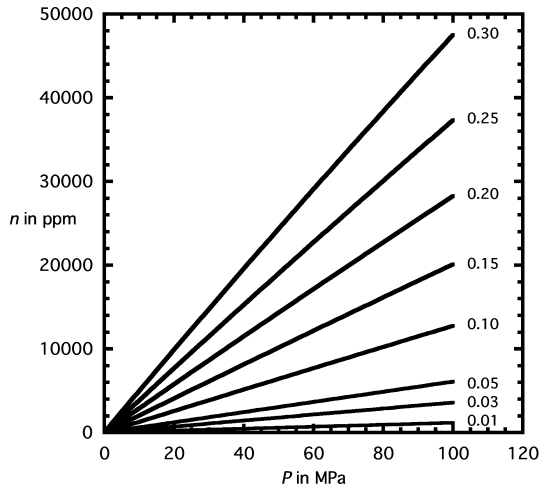

Fig. 2. Variation of the maximum mass fraction, n, of gas of molecular mass $m = 40$ kg kmol^{-1} that can be present in an asteroid as a function of the initial pressure in pore spaces or fractures, P, assumed to be lithostatic, for a range of values of the volume fraction, f, of pore spaces that are present (curves labeled by f as a volume fraction).

used above will underestimate their densities, causing the values of n in Fig. 2 to become significant underestimates at these large pressures. Clearly, for asteroids up to 100 km in diameter there is no difficulty in retaining up to 2000 ppm of gases, and asteroids of 4 Vesta size could have retained up to at least 50,000 ppm by mass (i.e., 5 mass%) of free volatiles at the onset of melting if these volatiles had been trapped during the accretion of the body. We stress, however, that there is no guarantee that trapping of gases in this way was common; the direct evidence from measurements suggests that volatile amounts were in the range 3000–9000 ppm for CO and up to 10,000–15,000 ppm for S_2. The calculations underlying Fig. 2 imply that there is no difficulty in understanding the retention of approximately 10,000 ppm of volatiles by large asteroids irrespective of how the volatiles are distributed, but that high volatile contents in small asteroids were most likely present in chemically bound, rather than free gas, form.

The initial melts that form as the temperature increases represent only a small fraction of the mass of the asteroid. However, it seems likely that much of the available trapped gas quickly makes contact with the liquids. In modeling the extraction of Fe,Ni–FeS melts from differentiated asteroids with compositions similar to H group ordinary chondrites, Keil and Wilson (1993) found that the initial Fe,Ni–FeS melts would represent up to approximately 5 mass% of the parent asteroid; thus dispersal of all of the trapped gases into these melts would give them gas contents up to 20 times greater than those in the bulk asteroid. However, calculations by Taylor (1992) suggested that Fe,Ni–FeS melt migration will not become efficient until after silicate melting begins. The theoretical modeling requires numerous assumptions which lead to great uncertainty in predicting accurately how much silicate melting is required to allow Fe,Ni–FeS melt migration to begin. Direct evidence comes from studies of the likely melt migration patterns in the acapulcoite–lodranite parent body (McCoy et al. 1997a, 1997b) which imply that approximately 20% silicate melting is required, implying that the bulk asteroid gas content would be enhanced by a factor of about four in the bulk melt mixture. We adopt this more conservative value and infer that the amount of free, as distinct from chemically bound, gas in the mixture of Fe,Ni–FeS and silicate melts, n_m, may have been typically up to 8000 ppm by mass in small asteroids but could have been up to 200,000 ppm in the largest differentiated bodies.

Next, we address the issue of the way gas will be distributed in melt rising toward the surface of an asteroid. The meteorite melting and degassing experiments described by Muenow et al. (1992) imply that at least some of the gases released from enstatite chondrites were physically bound to minerals rather than being present as gases in pore spaces. If melting occurs at a high enough pressure, volatile species present in either form may dissolve into the melt, to be released again as very small bubbles as the melt approaches the essentially zero pressure environment of the surface, thus mimicking the common pattern of gas release in volcanic activity on large planetary bodies. If the volatiles do not dissolve, they may accumulate into much larger gas bodies—gas "slugs." At the pressures near the center of a 100 km diameter body, approximately 3 MPa (Table 1), solubility measurements (Harris 1981; Gerlach 1986; Dixon 1997) show that silicate melts can dissolve approximately 2000–3000 ppm of relatively soluble species like H_2O and SO_2 and can retain approximately 20–30 ppm of relatively insoluble species like CO_2. Near the center of a Vesta-size asteroid, these values increase to approximately 25,000 and 600 ppm, respectively. Taken together with our above estimates of the amounts of free gas that can be retained in asteroids of various sizes and the measurements on meteorites as proxies for the parent lithologies of the differentiated meteorites in question, these results suggest that in both large and small asteroids undergoing volcanic activity we should be prepared to model the volatiles in melts approaching the surface as being both partly dissolved in the rising melts and partly present as free gas slugs.

DEVELOPMENT OF VOLCANIC SYSTEMS

We have explicitly assumed above that the pressure in the gas in pore spaces at the start of Fe,Ni–FeS melting was lithostatic. The increase in temperature from the asteroid accretion temperature to the Fe, Ni–FeS eutectic temperature will have tended to cause a pressure increase in the gas, but we have assumed that this increase was compensated by gas loss. This seems logical given that, if the gas was trapped at the local lithostatic pressure as the asteroid accreted, the approximately fivefold increase in temperature from the formation temperature, say 250 K, to the Fe,Ni–FeS eutectic melting temperature, approximately 1253 K, would have increased the gas pressure by the same factor of 5. The approximately 1 MPa pressure at the center of a 50 km diameter asteroid or at a depth of 10 km beneath the surface of an 80 km diameter body would have increased to 5 MPa, approaching the tensile strength of most silicate rocks (Jaeger and Cooke 1979) and causing fractures to form.

A potential additional source of pressure increase appears when melting begins. The density of the first melt to form, a Fe,Ni–FeS cotectic, is approximately 5100 kg m^{-3} (McCoy et al. 1997a, 1997b), whereas the average density of the Fe,Ni metal and FeS minerals that contribute to the melt (using density data from CRC 1972) is likely to be within ~5% of ~6500 kg m^{-3}. Thus, an approximately 20% volume increase occurs in the Fe,Ni–FeS liquid on melting. This volume is initially provided mainly by compression of the gas contained in pore spaces. However, as the pressure increases, compression of the solid and liquid phases present becomes important (Muenow et al. 1992). A similar process occurs when silicate melting starts, the volume increase being approximately 10%. Even small amounts of melting can readily produce a pressure increase of several tens of MPa throughout the interior of the asteroid (Muenow et al. 1992; Wilson et al. 2008). This increasing pressure will have caused the formation of new tensile fractures at all depths, rapidly evolving a network connecting the pre-existing pore spaces and fractures and promoting efficient melt and gas movement. Eventually, some of these new fractures will have propagated into and through the cold, brittle crustal shell, and as melt drained upward into them will have become dikes feeding surface eruptions as described by Wilson et al. (2008).

MELT MIGRATION

Assuming that significant silicate melting was required before efficient Fe,Ni–FeS liquid migration began (Taylor 1992; McCoy et al. 1997a, 1997b), there must commonly have been simultaneous migration of Fe,Ni–FeS liquid and silicate liquid. Buoyancy considerations alone would dictate that gas and liquid silicate would migrate upward whereas liquid Fe, Ni–FeS would migrate downward. However, with free gas present, at least some of the metal–sulfide melt pockets will have contained trapped gas bubbles, making them buoyant enough to be flushed up toward the surface and erupted along with silicate melts (Keil and Wilson 1993).

The presence of pockets of Fe,Ni–FeS liquid and its potential migration, either upward or downward depending on its gas bubble content, will have complicated the silicate fluid migration after silicate melting begins. The three fluid components, Fe,Ni–FeS melt, silicate melt, and free gas, are mutually immiscible, and so any movement of a bubble, droplet or slug of one phase relative to another phase will produce some kind of frictional drag force. Fortunately, the details of these interactions are not important to this study. This is because our concern is with the fate of pyroclasts produced when explosive eruptions occur at the surface. The large amount of energy available from the expansion of even a very small mass fraction of gas ensures that the speeds of the vast majority of the pyroclasts produced by magma disruption in explosive activity are much greater than the rise speed through the lithosphere of the predisruption magma (Wilson and Head 1981). As a result, the details of the ways in which interactions between Fe,Ni–FeS melt pockets, silicate melt pockets, and gas slugs influence the predisruption rise speed of the melts are largely irrelevant; the only important parameter is the mass fraction of gas in the liquid that reaches the vent (Wilson 1980).

Once dikes opened to the surface, a balance will have been established between the buoyancy forces coupled with excess melt pressure everywhere in the system and the flow rate of melt although the narrow veins and fractures at depth and in the dikes near the surface. Melt flow speed in such systems is controlled by a combination of the pressure gradient in the melt and the widths of the pathways; the pathway width is determined by the local total pressure, leading to a complex coupled system which will have tended toward an equilibrium in which the total silicate melt eruption rate just balanced the total silicate melt production rate, with the vein and dike network evolving to be compatible with this state. Wilson et al. (2008) describe the development of a volcanic system of this type in the ureilite parent body, the diameter of which they estimated as being between 82 and 128 km. They argued that incipient but poorly

developed Rayleigh-Taylor convective instabilities in the mantle would lead to the formation of a small number, probably approximately 5, of major networks of vein and fracture systems concentrating magma upward toward surface vents, each vent erupting on average 20 m^3 s^{-1} of silicate magma soon after melt formation began, the rate declining exponentially by a factor of approximately 20 over the ensuing 4 Ma. Melt production rates depend both on asteroid size and formation time for a given strength of the heat source. The earlier an asteroid forms, the greater will be the melt production rate at the start of melting and the longer the duration of activity. The arguments about incipient convective instability in asteroid mantles (Wilson et al. 2008) suggest that, although larger asteroids will produce a greater melt volume, they will also tend to develop a larger number of active volcanic centers, and so the eruption rate at a single vent may be less sensitive to asteroid size than to formation time.

Volume eruption rate at any given vent will directly influence lava flow lengths in effusive eruptions, on asteroids (Wilson and Keil 1996b) in the same way as on Earth (Pinkerton and Wilson 1994). It will also be a factor, along with eruption speed, in determining the thermal state of pyroclasts in explosive eruptions where the pyroclasts are retained on the asteroid to form cool pyroclastic cones or, more likely (Wilson and Keil 1997), hot lava ponds. However, we are concerned here with pyroclastic droplet size distributions, and whether droplets of a given size will achieve escape velocity. This is determined almost entirely by the gas content of the erupting gas–droplet mixture and by the way the magma disrupts to form the droplets. As described earlier, we expect in general that volatiles in melts nearing the surface will be present both in solution in the melts and as pockets of free gas forming slugs. The gas slugs may have a wide range of sizes, but as gases exsolve from decompressing melts they will form large numbers of small bubbles. This is because bubble nucleation energetics imply that bubbles will have initial radii of approximately 10 μm (Sparks 1978). These small bubbles will expand as the pressure decreases, but will have very small rise speeds in the surrounding liquids, both because of their small sizes and the low values of the acceleration due to gravity. There will thus be little opportunity for them to coalescence to form much larger bubbles. Clearly gas slugs are more likely to form when trapped gas that at no time has been dissolved in melts is present in the system. We now consider the ways in which each of these gas distribution states will control magma disruption to drive explosive eruptive activity.

MAGMA DISRUPTION MECHANISMS

Gas Dispersed As Small Bubbles

The eruption of a liquid containing small, dispersed gas bubbles into a vacuum has been modeled by numerous authors (Wilson and Head 1981, 2001, 2003; Kieffer 1982, 1984; Wilson and Keil 1991, 1996b, 1997; Muenow et al. 1992) and involves the expansion of bubbles of decompressing gas to form a foam that becomes unstable and disintegrates into a continuous gas phase transporting a spray of liquid droplets. In detail, the melt disruption process is complex, and is a function of the strain rate in the melt and the melt rheology, but for low-viscosity mafic melts it is commonly idealized by assuming that disruption occurs when the volume fraction of gas bubbles in the melt reaches a critical value of 0.75 (Sparks 1978). If this occurs at a pressure P_d, the gas density ρ_d will be given by

$$\rho_d = \frac{m P_d}{Q T_m}, \quad (4)$$

where T_m is the melt temperature. The liquid density, ρ_m, will depend on the proportions of silicate liquid and Fe,Ni–FeS liquid being erupted. We assume a weighted average of the component densities, $\rho_{sil} = \sim 3000$ and $\rho_{sul} = \sim 5100$ kg m^{-3}, respectively (McCoy et al. 1997a, 1997b). In modeling, the loss of Fe,Ni–FeS melt from a parent body to explain the sulfur content of the IVB iron meteorite group, Keil and Wilson (1993) estimated that about 88% of the Fe,Ni–FeS liquid must have been erupted. If, as assumed earlier, approximately 20% by mass silicate melting took place and approximately 5% by mass of Fe,Ni–FeS liquid was produced, and if 88% of the Fe,Ni–FeS was transferred upward with the silicate melt, the resulting 20:4.4 mass ratio implies a bulk melt density of $\rho_m = \sim 3380$ kg m^{-3}. The requirement that the partial volume occupied by the gas in the melt, proportional to (n_m/ρ_d), is three times the partial volume of the melt, proportional to $[(1 - n_m)/\rho_m]$, then leads to

$$P_d = \frac{Q T_m n_m \rho_m}{3 m (1 - n_m)}. \quad (5)$$

Table 2 shows values of P_d corresponding to a range of values of n_m; the temperature of the melt is set equal to 1500 K, corresponding to approximately 20% melting of the body. All of these pressures are small enough that the perfect gas law gives an accurate value for the gas density. Note that for large values of n_m the disruption pressure P_d is greater than the likely lithostatic pressures in the shallow mantles of asteroids smaller than approximately 100 km (see Table 1).

Table 2. Variation of eruption conditions with mass fraction of gas in erupted melts.

n_m	P_d	P_c	u_c	u_u	D_l
300	0.099	0.050	11.3	28.5	41.9
1000	0.330	0.167	20.6	52.0	76.6
1500	0.495	0.250	25.3	63.7	93.8
2000	0.660	0.334	29.2	73.5	108.3
3000	0.991	0.501	35.7	90.0	132.6
5000	1.655	0.837	46.1	116.2	171.2
10,000	3.328	1.682	65.2	164.4	242.1
20,000	6.723	3.397	92.3	232.5	342.4
50,000	17.339	8.761	145.9	367.6	541.4
100,000	36.605	18.496	206.3	519.8	765.6

Note: The melt is a mixture of sulfide and silicate liquids as discussed in the text; n_m is the mass fraction in ppm of gas in the melt; P_d is the gas pressure in MPa at which magmatic foam disrupts into droplets and free gas; P_c is the pressure at which the spray of droplets and gas is choked in the volcanic vent; u_c is the speed in m s^{-1} of the gas and small clasts at the choking point; u_u is the ultimate speed in m s^{-1} reached by the small droplets after gas expansion ends; D_l is the limiting diameter in km of the largest asteroid from which very small droplets moving at essentially the same speed as the gas can escape.

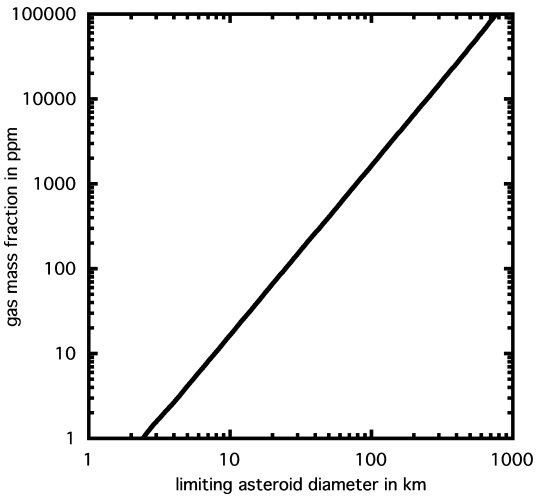

Fig. 3. Variation with asteroid diameter of the minimum gas mass fraction in an eruption required to eject the smallest pyroclasts into space with escape velocity.

Unless excess pressures exist in the melts in these asteroids, foams will not be stable, and segregation of gas into slugs will be very likely.

In eruptions on bodies without a significant atmosphere, a very rapidly widening vent system would be required to allow a smooth lateral expansion of the gas stream by the very great amount required to reach the extremely low final pressure in the expanding gas (Wilson and Head 1981; Kieffer 1982) and the flow at the level of the vent is much more likely to reach a choked condition (Kieffer 1982, 1984; Giberti and Wilson 1990) in which the speed of the gas phase and all small melt droplets (which have a negligible terminal fall velocity although the gas) is equal to the speed of sound in this compound fluid. The dependence of the sound speed on pressure and on droplet to gas mass ratio fixes the pressure at which this occurs. Above the vent, additional gas expansion and droplet acceleration occur although a series of shock waves, and eventually the gas pressure becomes so small that the perfect gas laws no longer apply; the system enters the Knudsen regime where collisions between gas molecules and droplets become more common than mutual collisions between gas molecules, and quickly the droplets become decoupled from the expanding gas to travel on ballistic paths in the weak gravity field.

Gas pressures, P_c, and speeds, u_c, of gas and entrained small clasts under the choked conditions in the vent can be found from the methods given as Equations 1–4 in Wilson and Head (2007) and Table 2 shows examples for a range of mass fractions n_m of a volatile with molecular mass $m = 40$ kg $kmol^{-1}$. Also given is the ultimate velocity, u_u, of the gas and small clasts after the gas expansion has reached the Knudsen regime. This is calculated by the method described by Wilson and Keil (1997), allowing the mixture of gas and small entrained droplets to expand adiabatically and decoupling the droplets from the gas, so that no further droplet acceleration occurs, when the mean free path of the gas molecules becomes equal to the typical droplet size. Equating u_u to the escape speed, u_e, from the surface of an asteroid of diameter D and density $\rho_a = 3300$ kg m^{-3}, given by

$$u_e = \left(\frac{2}{3}\pi G \rho_a\right)^{1/2} D \quad (6)$$

allows us to find, for a given volatile mass fraction, the limiting diameter, D_l, of the largest asteroid from which extremely small droplets moving at essentially the same speed as the gas can escape. These values are also given in Table 2 and plotted graphically in Fig. 3. Any volatile mass fraction in excess of approximately 1750 ppm will ensure the escape into space of all small droplets from asteroids 100 km in diameter, as found by Wilson and Keil (1991). However, much greater volatile contents are needed to eject pyroclasts from large asteroids: approximately 60,000 ppm, or 6% by mass, of gas would be needed to erupt even very small pyroclasts from 4 Vesta with escape velocity. We return to this issue in more detail later.

Gas Dispersed As Large Slugs

We now consider the situation where slugs of gas alternating with ribbons of liquid are erupted at the

surface instead of sprays of droplets in gas resulting from dispersions of bubbles in liquids. In this case, each ribbon of liquid will be surrounded by an expanding gas stream that will quickly accelerate to a much greater speed than the liquid ribbon. Such ribbons of liquid surrounded by rapidly moving gas are highly unstable, first developing wave-like instabilities along their length and quickly disintegrating into irregular droplets which themselves quickly disrupt into chains and clouds of secondary droplets. We develop the analysis for a silicate liquid and then discuss the differences caused by the much smaller viscosity of a Fe,Ni–FeS liquid.

If the liquid ribbons are approximated as having a circular cross sectional shape of radius R_r, the initial instabilities have a wavelength of $[(2\pi)/0.697]R_r = 9.02R_r$ (de Gennes et al. 2002). If each wave in the instability grows until the liquid within it pinches off from the liquid in the wave on either side, the pinched-off volume is $\pi {R_r}^2 \times 9.02R_r = 9.02\pi {R_r}^3$. If the pinched-off liquid contracts into a roughly spherical body of radius R_b, its volume is $(4/3)\pi {R_b}^3$, and as these volumes are equal, we find $R_b = [(3 \times 9.02)/4]^{1/3}R_r = 1.891R_r$. The subsequent break-up of these liquid bodies into secondary droplets can occur in a variety of modes that depend on the Weber number, *We*, and the Ohnesorge number, *Oh*. The Weber number is ratio of the inertial forces acting on a fluid to the surface tension of the fluid, and the Ohnesorge number is the ratio of the viscous force acting on the fluid to the geometric mean of the inertial and surface tension forces. The definitions of these dimensionless numbers in the present case are

$$We = \frac{\rho V^2 z}{\sigma} \tag{7}$$

and

$$Oh = \frac{\mu}{(\rho \sigma z)^{1/2}}, \tag{8}$$

where μ and ρ are the viscosity and density, respectively, of the liquid, σ is the surface tension of the liquid–gas interface, and z is a characteristic length in the liquid. V is the relative velocity of the gas and liquid; this will be essentially equal to the speed of the gas emerging from the vent, because the liquid ribbons will emerge at a much smaller speed than the gas; thus V will be a function of the mass fraction of gas, n_m. We take z to be the smallest cross sectional width of the primary liquid droplet into which the initial ribbon is disrupted, i.e., $z = 2R_b$.

Under these conditions, there are various possible modes of break-up of primary liquid bodies into secondary droplets, the three main ones being bag break-up, multimode break-up and shear break-up, and the relationships between them can be summarized (Schmehl 2003) by

$$3(1 + 15Oh^{1.2}) < We < 13(1 + 1.7Oh^{1.4}), \quad Oh < 0.3, \text{no breakup} \tag{9a}$$

$$13(1 + 1.7Oh^{1.4}) < We < 35(1 + 0.65Oh^{1.4}), \quad Oh < 4, \text{bag breakup} \tag{9b}$$

$$35(1 + 0.65Oh^{1.4}) < We < 80(1 + 0.6Oh^{1.3}), \quad Oh < 15, \text{multimode} \tag{9c}$$

$$80(1 + 0.6Oh^{1.3}) < We < \infty, \quad Oh < 6, \text{shear breakup} \tag{9d}$$

Table 3 shows the values of *We* and *Oh* relevant to the break-up of secondary silicate liquid drops of a very wide range of possible sizes ejected in eruptions with gas mass fraction of $n_m = 1000$ ppm, for which V is approximately 20 m s^{-1}. The melt–gas interface surface tension is taken as 0.4 Pa·m, a common value for mafic compositions (Walker and Mulins 1981; Philpotts and Carroll 1996), and the liquid density is $\rho = 3000$ kg m^{-3}. The viscosity, μ, is initially taken as 3 Pa·s, a plausible value for mafic silicate melts. The values of *Oh* are large enough to exert a significant influence on the ranges of *We* relevant to a given break-up mode, and so for each value of z and hence *We* we give the Weber numbers for the onset of each of the possible droplet break-up modes, together with the mode that actual occurs. Also given in the table are two estimates of the representative size of secondary droplets that form from the disrupted ribbons when disruption occurs, the Sauter mean diameter; D_{HF} is the form given by Hsiang and Faeth (1992) and D_S is the version suggested by Schmehl (2003):

$$D_{HF} = 6.2\, z\, \frac{Oh^{1/2}}{We^{1/4}} \tag{10a}$$

$$D_S = 1.5\, z\, Oh^{0.2} \left(\frac{1 + 1.7\, Oh^{1.4}}{We}\right)^{1/4} \tag{10b}$$

The results shown in Table 3 imply that the primary break-up of the liquid ribbons erupted by gas slugs will begin for all ribbon widths, and hence primary droplet diameters, greater than approximately 0.1 mm, although the sizes of the secondary droplets produced will be comparable to the sizes of their parent primary droplets. The entire spectrum of break-up

Table 3. Parameters related to volcanic liquid breakup on emerging from a vent.

z	We	Oh	Critical We, bag mode	Critical We, multimode	Critical We, shear mode	Actual breakup mode	D_{HF}	D_S
0.01	30	27.4	2287.8	2376.7	6959.2	None	0.14	0.05
0.03	90	15.8	1067.3	1120.3	3097.8	None	0.24	0.08
0.13	399	7.51	384.7	417.7	1067.8	Bag	0.51	0.16
0.23	675	5.77	270.3	299.8	745.9	Multi-	0.66	0.20
0.3	900	5.00	223.4	251.5	616.7	Shear	0.76	0.23
1	3000	2.74	103.6	128.2	297.5	Shear	1.4	0.42
3	9000	1.58	55.0	78.2	175.4	Shear	2.4	0.73
10	3×10^4	0.87	31.1	53.6	118.7	Shear	4.4	1.4
30	9×10^4	0.50	21.4	43.6	97.0	Shear	7.6	2.6
100	3×10^5	0.27	16.6	38.7	86.9	Shear	13.9	5.3
300	9×10^5	0.16	14.7	36.7	83.0	Shear	24.0	10.4
1000	3×10^6	0.09	13.7	35.7	81.2	Shear	43.8	22.4

Note: z is the typical width in mm of the primary droplets into which ribbons of emerging liquid disrupt when the liquid viscosity is 3 Pa·s and the gas mass fraction n_m is 1000 ppm; We and Oh are the dimensionless Weber and Ohnesorge numbers; the critical values of We for the onset of each of the possible bag, multi- and shear modes of breakup are given and the actual breakup mode is indicated; D_{HF} and D_S are two alternative estimates of the predicted mean sizes in mm of droplets produced by secondary liquid ribbon breakup, if it occurs.

modes is contained between primary droplet diameters of ~0.1 and ~0.3 mm; and for all primary droplets greater than approximately 0.3 mm in size, the secondary droplets formed in shear will be smaller than their parents. Furthermore, this size ratio increases with the primary ribbon and droplet scale: e.g., meter-size ribbons will disrupt into 20–30 mm secondary droplets.

These calculations are readily carried out for slug eruptions involving other gas contents and other liquid viscosities and densities. The finding that the full range of secondary break-up modes occurs over a narrow range of primary droplet sizes allows us to use the threshold primary droplet size for multimode break-up, z_m, which lies near the middle of the range, as a representative index of when break-up starts. For silicate melts with density 3000 kg m^{-3}, Fig. 4 shows how the onset of disruption characterized by multimode disruption varies with melt–gas content, n_m, and melt viscosity, μ. As an extreme example, Fig. 5 shows the corresponding Sauter mean secondary droplet diameter, D_S, which would be expected after the break-up of very large, meter-sized liquid ribbons. The major influence is clearly melt viscosity. Figure 6 shows an example of the variation with temperature of the viscosity of the silicate melt that would be produced on a body with a bulk composition like that of the enstatite chondrites, a likely composition for the parent body of the aubrite meteorites (e.g., Keil, Forthcoming). The viscosity was calculated over the solidus–liquidus temperature range approximately 1270–1770 K using the method of Giordano et al. (2008). In the early stages of silicate melting, the temperature will be a little higher than the solidus and we may expect the melt viscosity to be approximately 1000 Pa·s. Figure 4 then shows that all liquid ribbons and primary droplets larger than

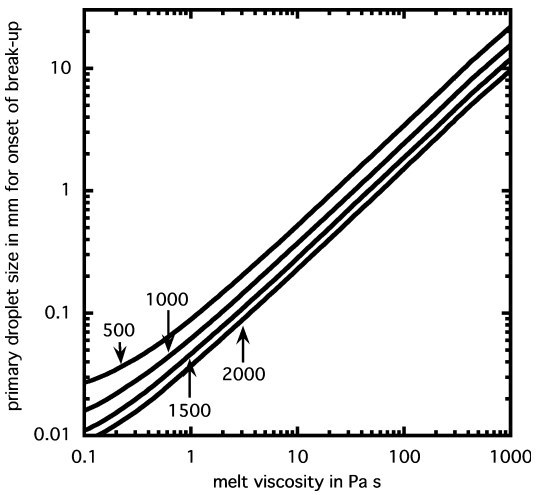

Fig. 4. Variation of primary droplet size at which break-up of silicate magma into smaller droplets begins as a function of magma viscosity and gas mass fraction in eruption products, labeled in ppm on curves.

approximately 10–20 mm in size will break up into smaller droplets. The secondary droplet size will vary with the primary droplet size, and again as an extreme example Fig. 5 shows that meter-size primary ribbons will produce secondary droplets that are approximately 200–300 mm in size. However, these secondary droplets will have a substantial terminal velocity in the accelerating gas, and so it is very likely that tertiary break-up will occur, further reducing the final droplet size. It must be recalled that silicate melting in asteroids differs from that in planets like the Earth (Wilson et al. 2008): in large planets solid-state convection in the mantle causes melting by adiabatic decompression—pressure-release melting—whereas in small asteroids

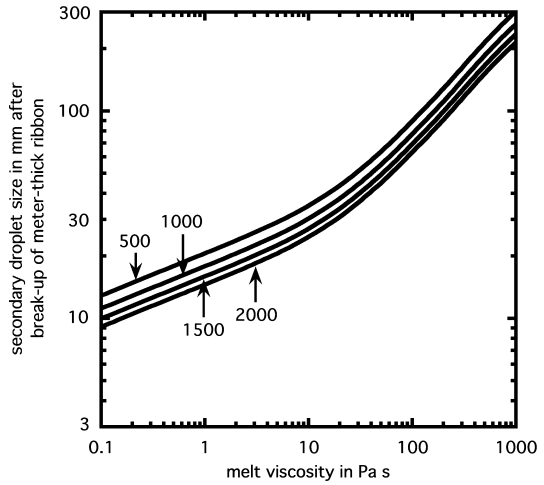

Fig. 5. Variation of secondary droplet size produced from the break-up of meter-sized primary ribbons of silicate magma as a function of magma viscosity and gas mass fraction in eruption products, labeled in ppm on curves.

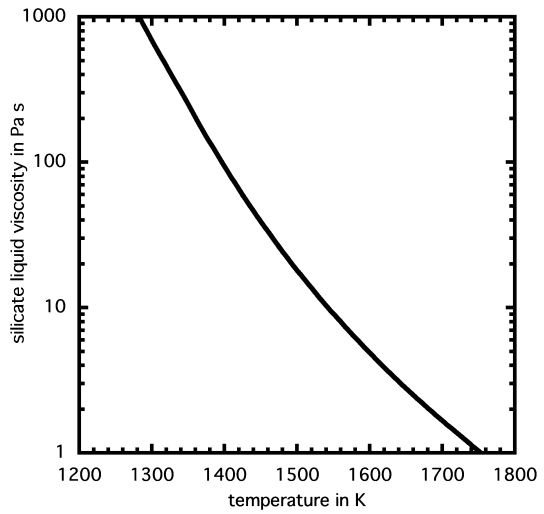

Fig. 6. Variation of silicate melt viscosity with temperature for the composition of the silicate component of the aubrite parent body.

mantle convection is negligible (Stevenson 2003; Wilson et al. 2008), and melting is entirely due to rising temperature. Thus, as silicate melting progresses, the temperature will increase and so the viscosity of the melt produced will progressively decrease. By the time, 50% silicate melting is reached and the viscosity reaches 3 Pa·s (see Fig. 6), all primary droplets larger than 0.1–0.2 mm will disrupt, and meter-sized ribbons and droplets will produce secondary droplets 15–25 mm in size, again with the potential for at least a small amount of further tertiary disruption. We stress that experience with measuring the pyroclast size distributions in mafic explosive eruptions on Earth, where gas expansion stops when the pressure reaches the atmospheric pressure of approximately 10^5 Pa, suggests that meter-thick ribbons of liquid are very rare (Parfitt 1998). There will be much greater expansion of gas in melts released into a vacuum, so only an extremely small fraction of the final droplets are likely to be as large as the sizes quoted here for meter-sized ribbons.

Fe,Ni–FeS melts have much smaller viscosities than silicate melts, typically approximately 10^{-2} Pa·s, but greater densities by a factor approaching 2. The functional dependencies of *Oh* and *We* on these parameters imply that the threshold size of ribbons and primary droplets for the break-up of Fe,Ni–FeS melts is about one half of the corresponding value for silicate melts of the same viscosity. The fact that the viscosity is approximately 100 times smaller for Fe, Ni–FeS melts than silicate melts implies that Fe, Ni–FeS liquid break-up is extremely efficient—even meter-size ribbons would quickly disrupt into approximately 5 mm droplets.

Overall, the conclusion of this part of analysis is that eruptions of gas slugs may produce some silicate pyroclastic droplets up to approximately 30 mm in size, but that droplets of this size and larger should be rare. The commonest sizes should be less than approximately 0.3 mm. Fe,Ni–FeS liquid droplets should generally be smaller than approximately 0.1 mm in size with rare examples up to a few mm. We now need to establish how the sizes of pyroclastic droplets produced in volcanic eruptions on asteroids influence whether they are able to acquire a large fraction of the speed of the erupting gases.

CONSEQUENCES OF FINITE SIZES OF PYROCLASTS

Direct evidence about the sizes of pyroclasts erupted into a vacuum comes from the lunar regolith samples returned by the Apollo missions: pyroclast diameters are almost always < 1 mm (e.g., Weitz et al. 1999). Similar or even smaller sizes are expected for pyroclastic droplets on asteroids as long as the gas is dispersed in the erupting liquid as small bubbles. The smallest magma disruption pressure shown in Table 2 is approximately 0.1 MPa. If gas bubbles nucleate with diameters of approximately 20 μm at the smallest (~0.5 MPa) and the largest (~130 MPa) of the internal asteroid pressures shown in Table 1, and decompress isothermally to the 0.1 MPa disruption pressure, they will expand by volume factors of ~5 and ~1300, respectively. The corresponding linear expansion factors are approximately 1.7 and 11, giving them diameters of approximately 34 and 220 μm, respectively. When a

foam consisting of such bubbles disintegrates, surface tension will tend to draw the irregular bodies of interstitial liquid into spherical droplets. The diameters of these droplets will depend on the geometry of close packing of the bubbles, but will be approximately 87–97% of the typical bubble size. Thus, we expect that eruptions on relatively large asteroids greater than approximately 100 km in diameter, where gas is present mainly as dispersed bubbles, will dominantly involve pyroclasts smaller than approximately 200 μm in diameter. In eruptions on asteroids less than approximately 100 km in diameter, where gas may be present mainly as slugs separating gas-free liquid, the pyroclastic droplets produced after liquid break-up will have a wide range of sizes but will mostly be < 0.3 mm in size, as found earlier.

In equilibrium, the amount by which the speed of a pyroclastic droplet lags behind the speed of the gas around it is equal to its terminal fall velocity, u_t, through the surrounding gas, readily obtained from the mutual drag force between the droplet and the gas. In addition to a dependence on droplet size and density, the terminal velocity is a function of the gas viscosity if the gas flow around the droplet is laminar and of the gas density if the gas flow is turbulent. The flow regime cannot be determined a priori, and the simplest approach is to find the terminal velocity using both assumptions and to check the Reynolds number implied by each for internal consistency, as described by Wilson and Keil (1997). For the largest pyroclasts considered, the flow regime is turbulent so that the terminal velocity u_t is given by

$$u_t = \left(\frac{4 \beta \rho_d g}{3 C_d \rho_g} \right)^{1/2}, \quad (11)$$

where β is the droplet diameter, ρ_d is the droplet density, ρ_d is the density of the expanding gas, g is the acceleration due to gravity, given by

$$g = \frac{2}{3} \pi G D \rho_a \quad (12)$$

and C_d is a drag coefficient with a value close to 0.7 for near-spherical pyroclasts (Wilson and Huang 1979). For small pyroclasts, the flow regime is laminar and the terminal velocity u_t is given by Stokes's law:

$$u_t = C_c \frac{\beta^2 \rho_d g}{18 \eta}, \quad (13)$$

where η is the viscosity of the gas, and C_c is a correction factor (Cunningham 1910) required when the gas density becomes very small and the mean free path of the molecules, λ, becomes comparable to the size of the pyroclastic droplets, i.e., the Knudsen regime is approached. C_c is given by (Allen and Raabe 1982, 1985)

$$C_c = 1 + Kn \left[2.34 + 1.05 \exp\left(\frac{-0.39}{Kn} \right) \right], \quad (14)$$

where Kn is the Knudsen number given by

$$Kn = \frac{2 \lambda}{d} \quad (15)$$

and λ is given by

$$\lambda = \frac{Q T_g}{\pi \varphi^2 N P_g}, \quad (16)$$

where ϕ is the effective diameter of the gas molecules. Values of ϕ do not vary in a systematic way with molecular mass, clustering between 3×10^{-10} and 4×10^{-10} m (Kaye and Laby 1995); we use $\phi = \sim 3.4 \times 10^{-10}$ m, which is close to the best estimate for both CO and N_2. N is Avogadro's number, 6.0225×10^{26} kmol^{-1}, and T_g and P_g are the temperature and pressure, respectively, in the expanding gas.

Table 4 shows how P_g, T_g, the gas speed u_g, the gas density ρ_g, the gas viscosity η, the molecular mean free path λ, the droplet terminal velocity u_t, and the actual speed of the droplet relative to the ground, $u_d = (u_g - u_t)$, vary during the gas expansion for a silicate liquid droplet of diameter 3 mm being erupted as part of a melt stream containing 1000 ppm gas. In the early stages of gas expansion, the terminal velocity of the droplet is small compared with the rapidly increasing gas speed and the droplet acquires a large fraction of the gas speed, reaching a maximum speed of ~ 57 m s^{-1}, about 88% of the ultimate ~ 65 m s^{-1} speed of the gas. As the gas becomes less dense and the Knudsen number increases above 0.1, the terminal velocity increases rapidly and, if inertia were to be ignored, the values of u_d in the last column would imply that the droplet would slow down again rapidly. However, by the time the Knudsen number has reached approximately 1, the drag force on the droplet will have become negligible. This 3 mm diameter droplet will therefore proceed on a trajectory determined by the only significant force still acting on it: the weak gravitational field of the asteroid. Equation 6 shows that the 57 m s^{-1} speed of this droplet is equal to the escape speed from an asteroid of radius approximately 42 km. Thus, a silicate droplet of this size would just be able to escape from any asteroid less than approximately 84 km in diameter, and all smaller droplets would escape with a finite velocity. The very smallest will have a speed essentially equal to the

Table 4. Parameter variations during the progressive expansion of a volcanic gas stream.

P_g	T_g	u_g	ρ_g	η	λ	Kn	u_t	u_d
217,770	1450	24.2	0.72257	49.1	0.0003	0.0002	1.15	23.10
110,038	1240	33.6	0.42694	44.9	0.0004	0.0003	1.29	32.35
55,601	1061	40.0	0.25213	41.0	0.0007	0.0005	1.42	38.55
28,095	907	44.7	0.14903	37.4	0.0012	0.0008	1.56	43.11
14,196	776	48.3	0.08802	34.0	0.0021	0.0014	1.71	46.62
7173	664	51.3	0.05197	30.8	0.0035	0.0023	1.89	49.37
3625	568	53.6	0.03070	27.9	0.0060	0.0040	2.09	51.54
1832	485	55.6	0.01817	25.1	0.0101	0.0067	2.33	53.25
925.4	415	57.2	0.01073	22.6	0.0171	0.0114	2.61	54.59
467.6	355	58.5	0.00634	20.2	0.0289	0.0192	2.94	55.60
236.3	304	59.7	0.00374	18.0	0.0489	0.0326	3.36	56.31
119.4	260	60.6	0.00221	16.0	0.0827	0.0551	3.89	56.73
60.3	222	61.4	0.00131	14.1	0.1400	0.0933	4.60	56.82
30.5	190	62.1	0.00077	12.4	0.2370	0.1580	5.62	56.47
15.4	163	62.7	0.00045	10.8	0.4011	0.2674	7.19	55.47
7.8	139	63.1	0.00027	9.4	0.6790	0.4527	9.86	53.29
3.9	119	63.6	0.00016	8.1	1.1493	0.7662	14.77	48.79
2.0	102	63.9	0.00009	6.9	1.9453	1.2969	24.22	39.69
1.0	87	64.2	0.00006	5.9	3.2928	2.1952	42.76	21.45
0.5	74	64.5	0.00003	5.0	5.5736	3.7158	79.53	—
0.3	64	64.7	0.00002	4.2	9.4343	6.2895	153.18	—

Note: P_g is the gas pressure in Pa; T_g is the gas temperature in K; u_g is the gas speed in m s^{-1}; ρ_g is the gas density in kg m^{-3}; η is the gas viscosity in units of 10^{-6} Pa·s; λ is the mean free path of the gas molecules in mm; Kn is the dimensionless Knudsen number for a 3 mm diameter pyroclastic droplet; u_t is the terminal fall velocity in m s^{-1} by which this droplet lags the gas speed; u_d is the droplet speed in m s^{-1} relative to the surface.

ultimate gas speed, in this case $\sim$65 m s^{-1}, $\sim$8 m s^{-1} greater than the escape speed.

This calculation has been repeated for other droplet sizes (and densities, to include Fe,Ni–FeS liquid droplets) and erupted gas mass fractions for asteroids of various sizes. Of particular interest is the critical droplet size which just achieves escape velocity on an asteroid of a given diameter; all droplets smaller than this size leave the asteroid with a finite speed and all droplets larger than this size fall back somewhere on its surface. For silicate droplets, Fig. 7 shows the variation of this critical pyroclast droplet size with asteroid diameter for a range of gas mass fractions in ppm. For the same asteroid size and gas fraction, the density difference means that Fe,Ni–FeS droplets would be a factor of 1.7 smaller.

Figure 7 reveals a number of relationships. Only a small amount of gas is needed to eject very large pyroclasts from small asteroids, but a very large amount is needed to eject even small pyroclasts from large asteroids. At their intersections with the abscissa, where they become nearly vertical, the curves define the minimum gas mass fraction that must be present in the melt to allow any, even the smallest, of the pyroclasts to be ejected from an asteroid of a given size. These intersections are, as expected, consistent with the values plotted in Fig. 3.

Furthermore, the size distribution of the pyroclasts is very important. Consider the vertical broken line in Fig. 7. This line is the asymptote to the 500 ppm gas curve and crosses the abscissa at an asteroid diameter of approximately 56 km. This implies that, on an asteroid with this size, essentially all pyroclasts, irrespective of their size, will be retained on the surface if the gas mass fraction, n_m, is 500 ppm or less. However, the vertical broken line crosses the curve for $n_m = 1000$ ppm at a pyroclast size of approximately 15 mm; this implies that on this 56 km diameter asteroid all pyroclasts will be ejected into space by 1000 ppm gas unless their diameter is >15 mm. Similarly the broken line crosses the curve for $n_m = 2000$ ppm at a clast size of 400 mm: if 2000 ppm gas is available in erupted melts on an asteroid 56 km in diameter, pyroclasts will have to be >400 mm in diameter to avoid being lost.

These findings mean that, if pyroclasts are identified as being present on the surface of a given asteroid, either directly by future spacecraft missions or by their recognition in meteorites, their sizes can in principle give information on the conditions in the eruption that formed them. If the asteroid size is known, or can be estimated indirectly, the size of the largest pyroclast gives a maximum estimate of the gas mass fraction involved in the eruption. For example, Fig. 7 shows that if a 10 mm silicate pyroclast is identified as being

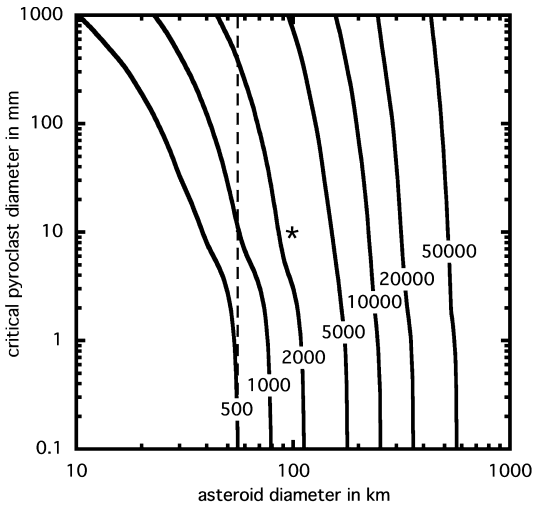

Fig. 7. Variation with asteroid diameter and erupted gas mass fraction, labeled on curves in ppm, of the critical size of silicate pyroclast that distinguishes smaller pyroclasts that are ejected at greater than escape velocity from larger pyroclasts that fallback onto the asteroid surface. Values correspond to $m = 40$ kg kmol^{-1}. The broken vertical line and the asterisk are used to illustrate specific relationships as discussed in the text.

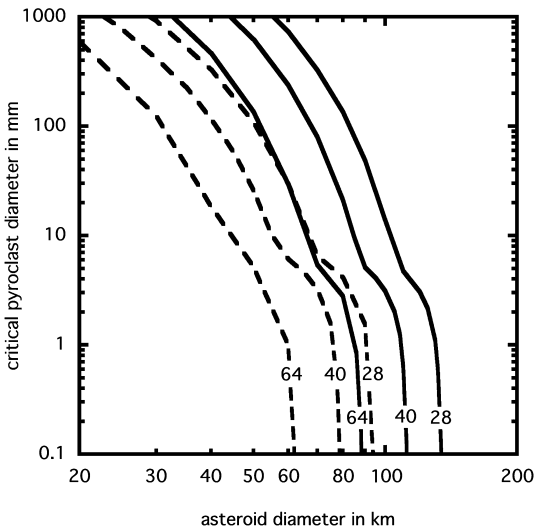

Fig. 8. The equivalent of Fig. 7 for $n = 1000$ ppm (broken curves) and $n = 2000$ ppm (solid curves) for each of $m = 28$, 40, and 64 kg kmol^{-1} (labels on curves).

present on a 100 km diameter asteroid, indicated by the asterisk, the gas mass fraction in the eruption that formed it must have been less than approximately 3000 ppm.

To derive the results shown in Fig. 7, a value of 40 kg kmol^{-1} was assigned to the molecular mass, m, of the gas to represent an average of the range of volatiles likely to be present, from $m = 28$ (CO) to $m = 64$ (S_2 or SO_2) kg kmol^{-1}. Repetition of all of the above calculations for values of m in this range shows that the position of the curves in Fig. 7 is quite strongly dependent on m. To illustrate this, Fig. 8 shows the equivalent of Fig. 7 for $n = 1000$ and 2000 ppm for each of $m = 28$, 40, and 64 kg kmol^{-1}; the horizontal scale is expanded for clarity. Fortunately, the functional dependencies between the variables, illustrated by Fig. 8, are such that Fig. 7 can be converted for use with any assumed or inferred volatile species by noting that the asteroid diameter D at which a given size pyroclast will have a speed equal to the escape speed is given to a good approximation by

$$D = K\left(\frac{n}{m}\right)^{1/2}, \tag{17}$$

where the constant K is equal to 16.3 km when n is expressed in ppm. Thus, the curves in Fig. 7 can be converted for use with other values of m by changing the numerical values on the asteroid diameter axis in inverse proportion to the square root of m.

SUMMARY AND DISCUSSION

We have explored how the dispersal of volatiles present as gases in asteroids influences the size distribution of pyroclasts produced in explosive eruptions driven by those gases, and we have then modeled the maximum velocities reached by pyroclasts of a given size and density on an asteroid of a given size as a function of the amount of gas released in the eruption. Comparison of the clast velocities with the escape velocity has allowed the critical pyroclast size that separates clasts retained on the surface from clasts lost to space to be determined as a function of asteroid diameter and gas content. Major conclusions are:

1. Asteroids greater than approximately 100 km in diameter are likely to have their gas dispersed mainly as small bubbles, the size distribution of which at the point of melt disruption causes most of the pyroclastic droplets produced to have diameters in the ~30 to ~200 μm range. It follows that vesicular meteorites in which the bulk of the vesicles are smaller than a few hundred μm in size are likely to have had parent bodies greater than approximately 100 km in diameter.
2. Asteroids less than approximately 100 km in diameter are likely to have their gas dispersed mainly as slugs rather than small bubbles, leading to a wider range of coarser droplet sizes on break-up of the liquid ribbons between the gas slugs; however, silicate pyroclast sizes are still expected to be mostly < 0.3 mm and almost always < 30 mm.
3. Asteroids less than approximately 100 km in diameter will erupt even very large pyroclasts with

more than escape velocity if quite modest amounts of gas are available. Conversely the ejection into space of even very small pyroclasts requires very large gas contents on asteroids larger than approximately 500 km, as shown by Fig. 3. This Figure implies that, for any plausible dissolved gas content (or gas mass fraction produced by smelting), volcanic ejection of pyroclasts becomes impossible on bodies a little smaller than the Earth's Moon.

4. Identification of the largest pyroclast present on an asteroid of a given size would provide a useful indicator of the maximum amount of gas of a given molecular mass that was involved in its eruption, as shown by Figs. 7 and 8.

We anticipate that these findings will be of value in interpreting the significance of volcanic clasts that may in the future be recognized in meteorites. They may also help in the interpretation of data from future generations of spacecraft missions either making soft-landings on the surfaces of differentiated asteroids or being able to identify the extents of pyroclastic deposits from orbit. The asteroid 4 Vesta is particularly relevant in view of the impending visit by the Dawn spacecraft. We have shown here that it is theoretically possible that a body of the size of 4 Vesta could have retained enough volatiles from the time of its accretion to allow even small pyroclasts erupted in the very earliest stages of its volcanic activity to be ejected with a velocity close to escape velocity. However, the composition of the HED meteorites suggests that 4 Vesta was not volatile-rich, and so it is very much more likely that the bulk of all products of explosive eruptions were retained on the body, as discussed by Wilson and Keil (1996b). These pyroclasts would most commonly have formed lava ponds around optically dense fire fountains, the cooled remains of which would have resembled lava flows as regards their physical properties (Wilson and Keil 1997). Nevertheless, these rocks might have retained the spectral characteristics (distinctive albedo and color) that have aided the identification of pyroclastic deposits on the Moon (Gaddis et al. 2003) and Mercury (Kerber et al. 2009). Only in the outermost parts of fire fountains on 4 Vesta are pyroclasts likely to have cooled sufficiently during flight to reach the ground as discrete glass beads, so the areas covered by such annular deposits would not be large. Nevertheless such clasts, which we predict should have diameters mainly in the ~30 to ~200 μm range, should exist, and might be detected spectroscopically from an orbiting or close fly-by spacecraft, although clearly detection from a soft-lander would be much less ambiguous.

Perhaps, the greatest source of uncertainty influencing the potential identification of volcanic materials on any asteroid is the impact history of the body. Some fortuitously located pyroclastic deposits on the Moon have survived more than 4 Ga of regolith and megaregolith development, but the smaller surface area of asteroids makes the chances of such favoured locations surviving smaller. It seems likely that the South Pole cratering event on Vesta (Thomas et al. 1997) would have lead to substantial resurfacing of the asteroid, and unfortunately this may have obscured any original pyroclastic deposits.

Acknowledgments— This work was supported in part by the NASA Cosmochemistry Program, grant NNX08AE08G (K. Keil, P.I.) and by grant NNG06GF56G (T. McCoy, P.I.). This is Hawaii Institute of Geophysics and Planetology Publication no. 1857, and School of Ocean and Earth Science and Technology Publication no. 7953.

Editorial Handling— Dr. Dina Prialnik

REFERENCES

Allen M. D. and Raabe O. G. 1982. Re-evaluation of Millikan's oil drop data for the motion of small particles in air. *Journal of Aerosol Science* 6:537–547.

Allen M. D. and Raabe O. G. 1985. Slip correction measurements of spherical solid aerosol particles in an improved Millikan apparatus. *Aerosol Science and Technology* 4:269–286.

Britt D. T., Yeomans D., Housen K., and Consolmagno G. 2002. Asteroid density, porosity, and structure. In *Asteroids III*, edited by Bottke W. F. Jr., Cellino A., Paolicchi P., and Binzel R. P. Tucson, AZ: The University of Arizona Press. pp. 485–500.

Burbine T. H., McCoy T. J., Meibom A., Gladman B., and Keil K. 2002. Meteorite parent bodies: Their number and identification. In *Asteroids III*, edited by Bottke W. F. Jr., Cellino A., Paolicchi P., and Binzel R. P. Tucson, AZ: The University of Arizona Press. pp. 653–667.

Carslaw H. S. and Jaeger J. C. 1959. *Conduction of heat in solids*, 2nd ed. New York: Oxford University Press. 510 p.

CRC 1972. *Handbook of chemistry and physics*, 53rd ed. Cleveland, OH: The Chemical Rubber Company. 2335 p.

Cunningham E. 1910. On the velocity of steady fall of spherical particles through fluid medium. *Proceedings of the Royal Society of London* 83:357–365.

Dixon J. E. 1997. Degassing of alkalic basalts. *American Mineralogist* 82:368–378.

Fogel R. 2005. Aubrite basalt vitrophyres: The missing basaltic component and high-sulfur silicate melts. *Geochimica et Cosmochimica Acta* 69:1633–1648.

Gaddis L. R., Staid M. I., Tyburczy J. A., Hawke B. R., and Petro N. E. 2003. Compositional analyses of lunar pyroclastic deposits. *Icarus* 161:262–280.

de Gennes P.-G., Brochard-Wyart F., and Quéré D. 2002. *Capillary and wetting phenomena—Drops, bubbles, pearls, waves*. New York: Springer.

Gerlach T. M. 1986. Exsolution of H_2O, CO_2, and S during eruptive episodes at Kilauea volcano, Hawaii. *Journal of Geophysical Research* 91:12,177–12,185.

Ghosh A., Weidenschilling S. J., McSween H. Y. Jr., and Rubin A. 2006. Asteroidal heating and thermal stratification of the asteroid belt. In *Meteorites and the early history of the solar system II*, edited by Lauretta D. S. and McSween H. Y. Jr. Tucson, AZ: The University of Arizona Press. pp. 555–566.

Giberti G. and Wilson L. 1990. The influence of geometry on the ascent of magma in open fissures. *Bulletin of Volcanology* 52:515–521.

Giordano D., Russell J. K., and Dingwell D. B. 2008. Viscosity of magmatic liquids: A model. *Earth and Planetary Science Letters* 271:123–134.

Goodrich C. A., Van Orman J., and Wilson L. 2007. Fractional melting and smelting on the Ureilite Parent Body. *Geochimica et Cosmochimica Acta* 71:2876–2895.

Harris D. M. 1981. The concentration of CO_2 in submarine tholeiitic basalts. *The Journal of Geology* 89:689–701.

Hsiang L.-P. and Faeth G. M. 1992. Near-limit drop deformation and secondary breakup. *International Journal of Multiphase Flow* 18:635–652.

Jaeger J. C. and Cooke N. G. W. 1979. *Fundamentals of rock mechanics*, 3rd ed. London: Chapman and Hall.

Kaye G. W. C. and Laby T. H. 1995. *Tables of physical and chemical constants*, 16th ed. London: Longman. 249 p.

Keil K. 1968. Mineralogical and chemical relationships among enstatite chondrites. *Journal of Geophysical Research* 73:6945–6976.

Keil K. 1989. Enstatite meteorites and their parent bodies. *Meteoritics* 24:195–208.

Keil K. 2007. Occurrence and origin of keilite, $(Fe_{>0.5},Mg_{<0.5})S$, in enstatite chondrite impact-melt rocks and impact-melt breccias. *Chemie der Erde—Geochemistry* 67:37–54.

Keil K. Forthcoming. Enstatite achondrite meteorites (aubrites) and the histories of their asteroidal parent bodies. *Chemie der Erde—Geochemistry*, doi:10.1016/j.chemer.2010.02.002.

Keil K. and Wilson L. 1993. Explosive volcanism and the compositions of cores of differentiated asteroids. *Earth and Planetary Science Letters* 117:111–124.

Keil K., Stöffler D., Love S. G., and Scott E. R. D. 1997. Constraints on the role of impact heating and melting in asteroids. *Meteoritics & Planetary Science* 32:349–363.

Kerber L., Head J. W., Solomon S. C., Murchie S. L., Blewett T., and Wilson L. 2009. Explosive volcanic eruptions on Mercury: Eruption conditions, magma volatile content, and implications for interior volatile abundances. *Earth and Planetary Science Letters* 285:263–271.

Kieffer S. W. 1982. Dynamics and thermodynmics of volcanic eruptions: Implications for the plumes on Io. In *Satellites of Jupiter*, edited by Morrison D. Tucson, AZ: The University of Arizona Press. pp. 647–723.

Kieffer S. W. 1984. Factors governing the structure of volcanic jets. In *Explosive volcanism: Inception, evolution and hazards*. Washington, D.C.: National Academy of Science Press. pp. 143–157.

Kullerud G. 1963. The Fe-Ni-S system. *Annual Reports of Geophysical Research* 67:4055–4061.

McCoy T. J. and Gale A. 2006. Pyroclastic volcanism on the aubrite parent body: Evidence from an Fe,Ni-FeS clast in LAR 04316 (abstract). *Meteoritics & Planetary Science* 41:A119.

McCoy T. J., Keil K., Clayton R. N., Mayeda T. K., Bogard D. D., Garrison D. H., Huss G. R., Hutcheon I. D., and Wieler R. 1996. A petrologic, chemical, and isotopic study of Monument Draw and comparison with other acapulcoites: Evidence for formation by incipient partial melting. *Geochimica et Cosmochimica Acta* 60:2681–2708.

McCoy T. J., Keil K., Clayton R. N., Mayeda T. K., Bogard D. D., Garrison D. H., and Wieler R. 1997a. A petrologic and isotopic study of lodranites: Evidence for early formation as partial melt residues from heterogeneous precursors. *Geochimica et Cosmochimica Acta* 61:623–637.

McCoy T. J., Keil K., Muenow D. W., and Wilson L. 1997b. Partial melting and melt migration in the acapulcoite-lodranite parent body. *Geochimica et Cosmochimica Acta* 61:639–650.

McCoy T. J., Mittlefehldt D. W., and Wilson L. 2006. Asteroid differentiation. In *Meteorites and the early solar system II*, edited by Lauretta D. S. and McSween H. Y. Jr. Tucson, AZ: The University of Arizona Press. pp. 733–745.

Mittlefehldt D. W., McCoy T. J., Goodrich C. A., and Kracher A. 1998. Non-chondritic meteorites from asteroidal bodies. In *Planetary materials*, edited by Papike J. J. Reviews in Mineralogy, vol. 36. Washington, D.C.: Mineralogical Society of America. pp. 4-1–4-195.

Muenow D. W., Keil K., and Wilson L. 1992. High-temperature mass spectrometric degassing of enstatite chondrites: Implications for pyroclastic volcanism on the aubrite parent body. *Geochimica et Cosmochimica Acta* 56:4267–4280.

Muenow D. W., Keil K., and McCoy T. J. 1995. Volatiles in unequilibrated ordinary chondrites: Abundances, sources and implications for explosive volcanism on differentiated asteroids. *Meteoritics* 30:639–645.

Nehru C. E., Prinz M., Weisberg M. K., and Delaney J. S. 1984. Parsa: An unequilibrated enstatite chindrite (UEC) with an aubrite-like impact melt clast (abstract). 15th Lunar and Planetary Science Conference. pp. 597–598.

Norris T. L., Gancarz A. J., Rokop D. J., and Thomas K. W. 1983. Half-life of ^{26}Al. *Journal of Geophysical Research* 88(Suppl. 1):B331–B333.

Nyquist E. L., Reese Y., Wiesmann H., Shih C. Y., and Takeda H. 2001. Dating eucrite formation and metamorphism. *Proceedings of the 26th Symposium on Antarctic Meteorites*. pp. 113–115.

Parfitt E. A. 1998. A study of size distribution, ash deposition and fragmentation in a Hawaiian-style volcanic eruption. *Journal of Volcanology and Geothermal Research* 84:197–208.

Philpotts A. R. and Carroll M. 1996. Physical properties of partly melted tholeiitic basalt. *Geology* 24:1029–1032.

Pinkerton H. and Wilson L. 1994. Factors controlling the lengths of channel-fed lava flows. *Bulletin of Volcanology* 56:108–120.

Schmehl R. 2003. *Tropfendeformation und nachzerfall bei der technischen gemischaufbereitung*. Dipl. Ing. Dissertation, University of Karlsruhe, Karlsruhe, Germany.

Shukolyukov A. and Lugmair G. W. 1993. Live Iron-60 in the early solar system. *Science* 259:1138–1142.

Sonett C. P., Colburn D. S., Schwartz K., and Keil K. 1970. The melting of asteroidal-sized parent bodies by unipolar dynamo induction from a primitive T Tauri sun. *Astrophysics and Space Science* 7:446–488.

Sparks R. S. J. 1978. The dynamics of bubble formation and growth in magmas: A review and analysis. *Journal of Volcanology and Geothermal Research* 3:1–37.

Srinivasan G., Goswani J. N., and Bhandari N. 1999. ^{26}Al in eucrite Piplia Kala: Plausible heat source and formation chronology. *Science* 284:1348–1350.

Stevenson D. J. 2003. Styles of mantle convection and their influence on planetary evolution. *Comptes Rendu Geoscience* 335:99–111.

Tachibana S. and Huss G. I. 2003. The initial abundance of ^{60}Fe in the solar system. *The Astrophysical Journal* 588:L41–L44.

Taylor G. J. 1992. Core formation in asteroids. *Journal of Geophysical Research* 97:14717–14726.

Thomas P. C., Binzel R. P., Gaffey M. J., Storrs A. D., Wells E. N., and Zellner B. H. 1997. Impact excavation on asteroid 4 Vesta: Hubble Space Telescope results. *Science* 277:1492–1495.

Urey H. 1955. The cosmic abundances of potassium, uranium and thorium and the heat balances of the Earth, the Moon and Mars. *Proceedings of the National Academy of Sciences* 41:127–144.

Walker D. and Mulins O. 1981. Surface tension of natural silicate melts from 1,200–1,500 °C and implications for melt structure. *Contributions to Mineralogy and Petrology* 76:455–462.

Warren P. H. 2010. The inevitability of a thick, strongly insulating megaregolith on bodies of order 100-km to Moon-like in size (abstract #2465). 41st Lunar and Planetary Science Conference. CD-ROM.

Warren P. H. and Kallemeyn G. W. 1992. Explosive volcanism and the graphite-oxygen buffer on the parent asteroid(s) of the ureilite meteorites. *Icarus* 100:110–126.

Weitz C. M., Rutherford M. J., Head J. W., and McKay D. S. 1999. Ascent and eruption of a lunar high-titanium magma as inferred from the petrology of the 74001/2 drill core. *Meteoritics & Planetary Science* 34:527–540.

Whittington A. G., Hofmeister A. M., and Nabelek P. I. 2009. Temperature-dependent thermal diffusivity of the Earth's crust and implications for magmatism. *Nature* 458:319–321.

Wilson L. 1980. Relationships between pressure, volatile content and ejecta velocity in three types of volcanic explosion. *Journal of Volcanology and Geothermal Research* 8:297–313.

Wilson L. and Head J. W. 1981. Ascent and eruption of basaltic magma on the Earth and Moon. *Journal of Geophysical Research* 86:2971–3001.

Wilson L. and Head J. W. 2001. Lava fountains from the 1999 Tvashtar Catena fissure eruption on Io: Implications for dike emplacement mechanisms, eruption rates and crustal structure. *Journal of Geophysical Research* 106:32997–33004.

Wilson L. and Head J. W. 2003. Deep generation of magmatic gas on the Moon and implications for pyroclastic eruptions. *Geophysical Research Letters* 30:1605.

Wilson L. and Head J. W. 2007. Explosive volcanic eruptions on Mars: Tephra and accretionary lapilli formation, dispersal and recognition in the geologic record. *Journal of Volcanology and Geothermal Research* 163:83–97.

Wilson L. and Huang T.-C. 1979. The influence of shape on the settling velocity of volcanic ash particles. *Earth and Planetary Science Letters* 44:311–324.

Wilson L. and Keil K. 1991. Consequences of explosive eruptions on small Solar System bodies: The case of the missing basalts on the aubrite parent body. *Earth and Planetary Science Letters* 104:505–512.

Wilson L. and Keil K. 1996a. Clast sizes of ejecta from explosive eruptions on asteroids: Implications for the fate of the basaltic products of differentiation. *Earth and Planetary Science Letters* 140:191–200.

Wilson L. and Keil K. 1996b. Volcanic eruptions and intrusions on the asteroid 4 Vesta. *Journal of Geophysical Research* 101:18927–18940.

Wilson L. and Keil K. 1997. The fate of pyroclasts produced in explosive eruptions on the asteroid 4 Vesta. *Meteoritics & Planetary Science* 32:813–823.

Wilson L., Goodrich C. A., and Van Orman J. A. 2008. Thermal evolution and physics of melt extraction on the Ureilite Parent Body. *Geochimica et Cosmochimica Acta* 72:6154–6176.

Wu S.-C. and Browne E. 1998. *Comments on evaluation of 26Al electron capture and positron decay data. CEA/LNHB—Table de Radionucléides*. Saclay, Gif-sur-Yvette, France: LNE-LNHB, CEA.

DEFINITIONS OF SYMBOLS

C_c	Cunningham correction factor
C_d	Dimensionless drag coefficient in turbulent flow, approximately 0.7
D	Diameter of asteroid
D_l	Limiting asteroid diameter from which small droplets can escape
D_{HF}	Sauter mean diameter of secondary liquid droplets (Hsiang and Faeth 1992)
D_S	Sauter mean diameter of secondary liquid droplets (Schmehl 2003)
G	Universal gravitation constant, 6.67×10^{-11} m^3 s^{-2} kg^{-1}
K	Constant in Equation 17
Kn	Knudsen number
N	Avogadro's number, 6.0225×10^{26} kmol^{-1}
Oh	Ohnesorge number
P	Pressure at any depth in asteroid
P_c	Pressure in vent of choked flow eruption
P_d	Pressure at which melt–gas mixture disrupts into gas–droplet spray
P_g	General pressure in expanding gas
P_0	Pressure at center of asteroid
P_{10}	Pressure at 10 km depth in asteroid
Q	Universal gas constant, 8.314 J mol^{-1} K^{-1}
R_b	Radius of liquid body formed from liquid ribbon breakup

(*Continued*)

R_r	Equivalent radius of erupted liquid ribbon
T_g	General temperature in expanding gas
T_m	Temperature of silicate–sulfide melt mixture
T_s	Temperature of start of sulfide melting, 1250 K
V	Relative velocity of gas and liquid slugs
We	Weber number
d	Depth below surface of asteroid
f	Volume fraction of pore space in asteroid
m	Mean molecular mass of asteroid volatiles
n	Asteroid mass fraction consisting of trapped volatiles
n_m	Mass fraction of gas in erupted mixture of sulfide and silicate melts
u_c	Speed of gas and small clasts in vent under choked conditions
u_d	General speed of droplet during its acceleration
u_e	Escape speed from surface of asteroid
u_g	Speed of expanding gas
u_t	Terminal velocity of pyroclasts in entraining gas
u_u	Final eruption speed of gas and small pyroclasts
v_g	Partial volume of asteroid that is gas
v_s	Partial volume of asteroid that is solids
z	Characteristic length scale in disrupting liquid bodies
z_m	Threshold primary droplet size for multimode break-up
β	Diameter of pyroclastic droplet
η	Viscosity of erupting gas phase
κ	Thermal diffusivity of the asteroid rock, 10^{-6} m^2 s^{-1}
λ	Mean free path of gas molecules
μ	General melt viscosity
ϕ	Effective diameter of gas molecules
ρ	General melt density
ρ_a	Mean bulk density of asteroid solids, 3300 kg m^{-3}
ρ_d	Density of gas when melt disruption occurs
ρ_g	Density of asteroid volatile gas
ρ_m	Bulk density of mixture of silicate and sulfide liquids, 3170 kg m^{-3}
ρ_{sil}	Density of silicate liquid, 3000 kg m^{-3}
ρ_{sul}	Density of sulfide liquid, 5100 kg m^{-3}
σ	Surface tension of gas–liquid interface, approximately 0.4 Pa·m
τ	Time since asteroid formation